Applied Surface Science 454 (2018) 327–333

Contents lists available at ScienceDirect

Applied Surface Science

journal homepage: www.elsevier.com/locate/apsusc

Full Length Article

Manipulation of multiple periodic surface structures on metals induced by femtosecond lasers

Hyun Uk Lim[a,b], Jeongjin Kang[a], Chunlei Guo[c,d], Taek Yong Hwang[a,*]

[a] Molds & Dies R&D Group, Korea Institute of Industrial Technology, Bucheon 14441, South Korea
[b] Department of Mechanical Engineering, Dankook University, Yongin 16890, South Korea
[c] The Institute of Optics, University of Rochester, NY 14627, USA
[d] The Guo China-US Photonics Laboratory, Changchun Institute of Optics, Fine Mechanics, and Physics, Changchun, China

ARTICLE INFO

Keywords:
Femtosecond phenomena
Laser-induced surface structure
Metal
Nanostructure fabrication
Light-matter interaction
Effective medium theory

ABSTRACT

Under femtosecond laser pulse irradiation, the selective control of structural periods of low spatial frequency laser-induced periodic surface structures (LSFLs) is investigated on metals at large incident beam angles. As increasing the number of irradiating pulses, we produce three types of LSFLs, small-, dual-, and large-scale LSFLs, and find two kinds of structural period variations, the sequential structural variations from small- to dual- to large-scale LSFLs and the nonsequential variation directly from small- to large-scale LSFLs by controlling the laser fluence. Using the efficacy factor with the help of the Maxwell-Garnett theory, our study also shows that all three types of LSFLs can be understood by the interference between the incident beam and surface plasmon polaritons at the air-nanostructure composite and metal interface rather than the air-metal interface.

1. Introduction

Since their first observation, laser-induced periodic surface structures (LIPSSs) have been investigated on various materials by using numerous types of high power lasers over the past half a century, and it is now generally considered that the formation of LIPSSs following laser irradiation is regarded as one of universal phenomena in laser-matter interaction [1–14]. In the past decades, LIPSSs have been actively investigated with femtosecond (fs) laser pulse irradiation [11–22]. Compared to the LIPSSs produced with relatively long pulsed lasers, fs LIPSSs generally show significantly reduced periods, and typically have been categorized into two distinct types, high spatial frequency LIPSSs (HSFLs) and low spatial frequency LIPSSs (LSFLs), where their periods are less than λ/2 (λ :laser wavelength) and between λ/2 and λ at normal incidence, respectively [11,19]. Occasionally, fs LIPSSs with a period of larger than λ have been also reported [23]. For HSFLs, various formation mechanisms such as second/third harmonic generation [5,20,24], surface oxidation [20], self-organization [25], and cavitation instability [26,27] have been suggested on various materials depending on their periods and orientations [5,11,14,20,24–26]. Recently, due to the observations of near- and sub-100 nm HSFLs, the formation mechanisms of HSFLs are still actively investigated [11,20,26]. On the other hand, the formation mechanism of LSFLs on metals is rather well understood by nonuniform periodic heating of surface due to the interference between the incident laser pulse and the laser excited surface plasmon polaritons (SPPs) with the adjustments of dielectric constant by considering laser-induced carrier excitations for semiconductors [17,18,24] and extensive surface nanostructures including the groove of LSFLs itself for metals [15,16,18,22]. Currently, by using the two temperature model, more sophisticated simulations have been performed for LSFLs [21,28].

According to the interference mechanism, particularly at off normal incidence, LSFLs on metals can intrinsically have two distinguishable structural periods, large- and small-scale periods, depending on the propagating direction of SPPs that interfere with the incident beam [3]. In case the incident beam interferes with SPPs propagating along the incident beam, the period of LSFLs will increase with the incident beam angle, and decrease when SPPs propagate against the incident beam along the air-metal interface [3,16]. Previously at off normal incidence, the former type of LSFLs (large-scale LSFLs) was observed on metals by us [16], and several observations were available by others for both the former and latter types of LSFLs (small- and large-scale LSFLs) on metals and semiconductors with various incident beam angles [13,29–31]. Recently, we observed structures with dual periods, namely dual-scale LSFLs, where the former and latter types of LSFLs coexist at the surface of metals [32]. The control of incident beam angle can give us an additional degree of freedom to change the period of LSFLs [3,16]. With this capability, it is also expected to efficiently fabricate the surface of

* Corresponding author.
E-mail address: taekyong@kitech.re.kr (T.Y. Hwang).

https://doi.org/10.1016/j.apsusc.2018.05.158
Received 5 March 2018; Received in revised form 15 May 2018; Accepted 21 May 2018
Available online 22 May 2018

polymer with various optical and physical properties, since LSFLs on metals including Ni can be easily replicated at the surface of polymer [33]. Therefore, to fully make use of these benefits, it is necessary to have a capability of independently selecting either one or both of two structural periods. However, currently, it is not clear how to pick out a specific scale of LSFLs' period with the number of irradiating pulses.

In this paper, by irradiating femtosecond (fs) laser pulses on metals, we manipulate the structural period of LSFLs at large incident angles. By adjusting the number of irradiating fs laser pulses, we fabricate small-, dual-, and large-scale LSFLs on metals, and demonstrate two kinds of structural period variations, the sequential structural variations of these three types of LSFLs and the nonsequential variation directly from small- to large-scale LSFLs with the control of laser fluence. We also discuss that all structural periods of LSFLs described here are attributed to the interference between the incident beam and SPPs travelling in the two opposite directions along the air-nanostructure composite and metal interface.

2. Methods and materials

Our experiments employ a Ti:sapphire laser system that generates 120-fs with the maximum pulse energy of 5 mJ/pulse and operates with a central wavelength of 800 nm at a 1 kHz repetition rate. The samples used in our experiments were Ni foils with a thickness of 1 mm, and prepared by polishing the surfaces mechanically with 80-nm-grade colloidal silica, and the average roughness (Ra) of polished surfaces was 9.4 nm. P-polarized fs laser pulses were slightly focused onto the surface of samples with a lens with a focal length of 150 mm, and the sample was slightly moved towards the lens to minimize nonlinear optical effects of air. The sample was vertically mounted on a rotation stage to produce LSFLs at off normal incidence. The $1/e^2$ intensity spot size (radius) is used to estimate the fluence of laser. The number of irradiating pulses is carefully adjusted with an electro-mechanical shutter, and the laser fluence is controlled by using a polarizer and half wave plate assembly. All experiments are performed in ambient air, and the period and morphological profile of LSFLs are measured by using a scanning electron microscope (SEM) and atomic force microscope (AFM), respectively.

3. Results and discussion

By irradiating the surface of Ni with fs laser pulses at a fluence (F) of 0.11 J/cm^2, we produce LSFLs at an incident angle of 65°. Following 10 pulses of irradiation, LSFLs form only in a small area within the beam spot. The period of LSFLs is about 415 nm, and the grating vector of LSFLs is parallel to the tangential component of laser polarization, as shown in Fig. 1. The structured area continuously expands with the number of irradiating pulses. Depending on the number of pulses, the period of LSFLs observed within the spot is in a range of 310–415 nm. The period decreases with the number of irradiating pulses, as described in Figs. 1 and 2. The LSFLs are covered with a large amount of nanoscale surface structures. These are consistent with the previous observations at normal incidence [15,18]. Comparing Fig. 1 with Fig. 2, we also notice that the shape of nanoscale structures covering LSFLs is changed from randomly oriented nanostructures (nanoscale protrusions, rims, and spheres etc.) to smaller porous type surface structures with the number of pulses.

Next, the fluence of laser is elevated to 0.17 J/cm^2 by increasing the pulse energy while other conditions are fixed, and the evolution of LSFLs is monitored with the number of irradiating pulses. At this fluence, the period of LSFLs is distributed in a range of about 350–415 nm, and the orientation of LSFLs is the same as that of LSFLs produced at lower laser fluence. The type of nanostructures on LSFLs is randomly oriented nanostructures, and the size of these nanostructures tends to increase with the number of pulses, as shown in Fig. 3(a)–(e). At this fluence, the change of nanostructure type to the porous type surface

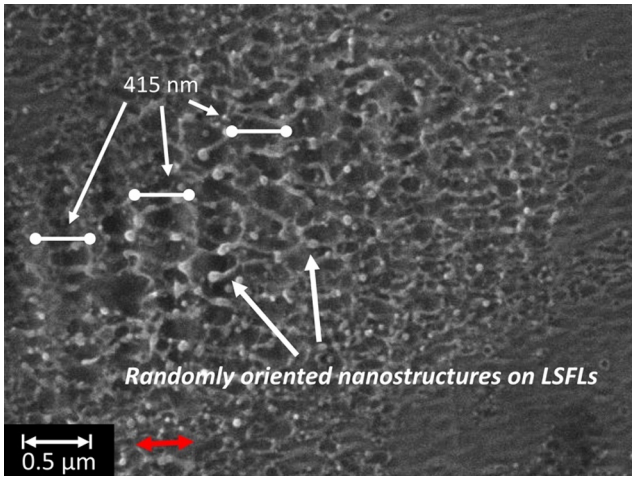

Fig. 1. SEM images of small-scale LSFLs on Ni produced at a fluence of 0.11 J/cm^2 and an incident angle of 65° with 10 pulses of irradiation. Double-headed arrows (red) indicate the orientation of polarization.

structures observed at $F = 0.11$ J/cm^2 slightly appears only at 50 pulses of irradiation, as shown in the inset of Fig. 3(b); however, with larger pulse numbers, this change is not shown. No significant change in the LSFLs' period is also observed up to 100 pulses of irradiation, as shown in Fig. 3(a)–(c); however, as the number of pulses reaches 250 pulses, the first structural period variation starts to happen, and large-scale LSFLs come into view along with small-scale LSFLs initially produced at lower pulse numbers. The period of large-scale LSFLs is in a range of 2.1–2.9 μm, more than 5 times larger than that of small-scale LSFLs, as described in Fig. 3(d). Until the number of pulses reaches 500, both small- and large-scale LSFLs, namely dual-scale LSFLs, clearly coexist on Ni, as shown in Fig. 3(d) and Ref. [32]. We also perform the similar experiments on Cu and Ag at larger incident angles of 70° and 80°, and observe dual-scale LSFLs on these metals. With additional 500 pulses of irradiation, dual-scale LSFLs on Ni experience another structural variation, resulting in vanishing small-scale LSFLs, and large-scale LSFLs are covered only with randomly oriented nanostructures, as shown in Fig. 3(e). By increasing the number of pulses, we can observe the sequential structural variations of small- to dual- to large-scale LSFLs within a fluence range of 0.14–0.17 J/cm^2.

We further increase the fluence of laser to 0.24 J/cm^2. In the beginning with low pulse numbers, the period of small-scale LSFLs is around 370–420 nm. Compared with LSFLs at $F = 0.17$ J/cm^2, no clear difference in the shape and orientation of small-scale LSFLs is observed below 100 pulses of irradiation; however, with more pulses of irradiation, the small-scale LSFLs start losing their periodic nature, and are completely gone prior to the formation of large-scale LSFLs, as shown in Fig. 3(f)–(h). Due to this early disappearance of small-scale LSFLs with low pulse numbers, small- to large-scale LSFLs direct transition with no dual-scale LSFL stage, namely the nonsequential structural variation, occurs at relatively high laser fluence.

When we take a look at Fig. 3(a)–(d) and (f)–(h), there seem some nanoscale quasiperiodic structures oriented perpendicular to small-scale LSFLs. Combined with small-scale LSFL structures, these structures form an array of rectangular domain at the surface. However, under identical experimental conditions, the period of these structures varies a lot and is not well-defined. As shown in the insets of Fig. 3, the shape of these structures are very similar to randomly oriented nanostructures described in Fig. 1 and Ref. [34,35]. As discussed in Ref. [34], their average distance also tends to increase with the pulse number and laser fluence. Accordingly, it is expected that the formation of these quasiperiodic structures results potentially from squirting liquid metal within a pot of locally melted liquid metal due both to Marangoni force and recoil pressure [34,35]. The reason that these randomly oriented

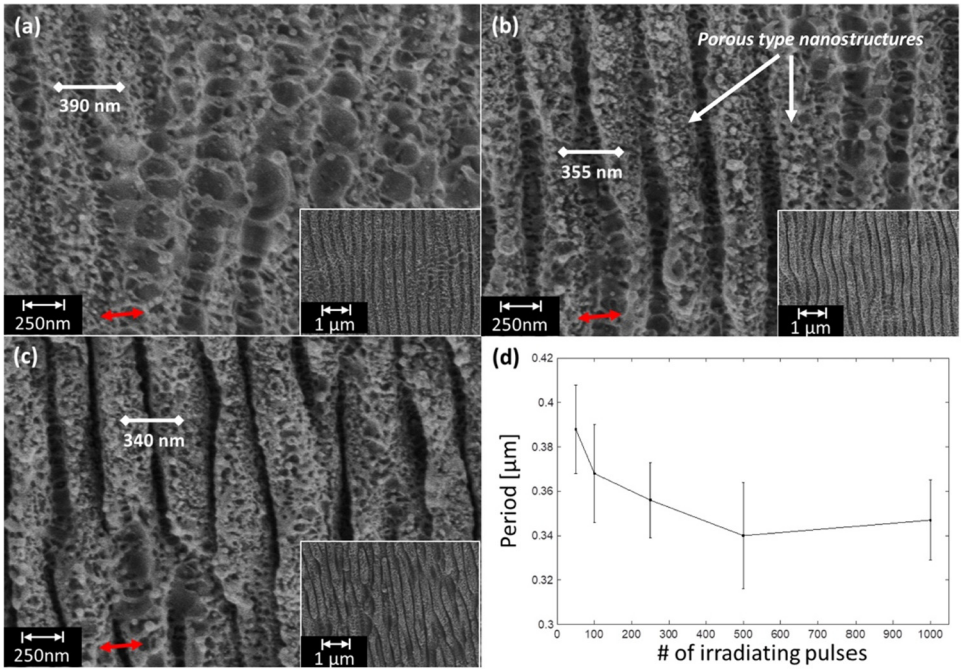

Fig. 2. SEM images of small-scale LSFLs on Ni produced at a fluence of 0.11 J/cm^2 and an incident angle of 65° with (a) 50 pulses, (b) 250 pulses, and (c) 1000 pulses of irradiation. (d) The period of LSFLs vs the number of irradiating pulses. Double-headed arrows (red) indicate the orientation of polarization.

nanostructures look rather well-aligned along the vertical direction in Fig. 3 is due to small-scale LSFLs. As clearly seen in Fig. 3(e), (i), and (j), this alignment is almost gone without small-scale LSFLs.

Let us start to discuss the formation mechanism of the observed periods of small-, dual-, large-scale LSFLs. As briefly discussed earlier, nonuniform periodic heating of surface following the interference between the incident beam and SPPs is attributed to the formation of LSFLs on metals. In fact, this interference mechanism is consistent with the Sipe's theory for the formation of LIPSSs [3]. Accordingly, by introducing so-called efficacy factor, this theory has successfully predicted the period of LSFLs produced with relatively long pulsed lasers, where the period of structures is positioned at the peak of the efficacy factor [3].

To apply the efficacy theory to our experimental results on LSFLs, we only consider a p-polarized laser pulse, and the grating vector of LSFLs is in the line of intersection of two planes, the plane of incidence and the surface of metal. Under these limited conditions, the resonance or peak position of the efficacy factor at the air-metal interface will be simply determined by the following equation [3]:

$$\omega_0(\kappa, \kappa_i)\varepsilon + \omega(\kappa, \kappa_i) \cong 0 \quad (1)$$

where κ is the wave number of LIPSSs, κ_i ($=2\pi\sin\theta/\lambda$) is the tangential component of wave number of incident light, θ is the incident angle, λ is the wavelength of incident light, $\omega_0 = [(2\pi/\lambda)^2 - (\kappa \pm \kappa_i)^2]^{1/2}$, $\omega = [(2\pi/\lambda)^2\varepsilon - (\kappa \pm \kappa_i)^2]^{1/2}$, and ε is the dielectric constant of metal.

As mentioned earlier in Section 1, the periods of LSFLs produced with multiple pulses of fs laser irradiation are significantly smaller than the ones expected from the efficacy factor due to the prompt change in the optical constant of materials [17,18,24,36], extensive randomly oriented surface nanostructures [15,16], and the grooves of LSFLs [18,22]. However, under our experimental conditions, the prompt change in the optical constant of Ni does not play a decisive role to reduce the LSFLs period, since the period of LSFLs on Ni is nearly the same as its theoretical value of 417 nm, obtained by using the tabular value of optical constant of Ni [37], at the initial stage of LSFLs formation with 10 pulses of irradiation, as shown in Figs. 1, 3(a) and (f). Moreover, it is noticed from Figs. 2 and 3 that the rate of decrease in the LSFLs period with the irradiating pulses diminishes at relatively higher fluences.

To consider the effects from these surface structures, we assume nanostructures on LSFLs as a thin layer of air-nanostructure composite that consists of air host and metal inclusion, described in Fig. 4(a) and our previous study [16]. With the help of the Maxwell-Garnett theory of effective media [38,39], the effective dielectric constant of air-nanostructure composite can be quantitatively evaluated as a function of volume fraction of metal inclusion by using dielectric constants of $1 + 0i$ (air) and $-19 + 21.7i$ (Ni) [37]. As shown in Fig. 4(b), both the real and imaginary parts of effective dielectric constant of the composite layer monotonically increase from the dielectric constant of air ($\approx 1 + 0i$) with the volume fraction of Ni inclusion.

With our assumption described above, the interference can occur at the surface of air-nanostructure composite layer and/or the surface of bulk metal. However, SPPs cannot be excited by the incident light at the interface between air and air-nanostructure composite layer, since the real part of dielectric constant of air-nanostructure composite layer is positive [40], as shown in Fig. 4(b). Therefore, we can simply rule out this possibility, and consider the remaining possibility that the interference happens at the interface between the air-nanostructure composite layer and bulk metal, described in Fig. 4(a). Accordingly, the modification of Eq. (1) is unavoidable because Eq. (1) is only applicable at the air-metal interface.

Actually, Eq. (1) is originated from the denominator of Fresnel equations [41]. We simply replace Eq. (1) with $\omega_0'(\kappa, \kappa_i)\varepsilon_{metal} + \omega'(\kappa, \kappa_i)\varepsilon_{eff} \cong 0$, obtained from the denominator of Fresnel coefficient at the composite layer-metal interface with the dielectric constants of air-nanostructure composite layer (ε_{eff}) and metal (ε_{metal}). ω_0' and ω' are defined as $[(2\pi/\lambda)^2\varepsilon_{eff} - (\kappa \pm \kappa_i)^2]^{1/2}$ and $[(2\pi/\lambda)^2\varepsilon_{metal} - (\kappa \pm \kappa_i)^2]^{1/2}$, respectively [41]. After arranging this replaced equation, we can obtain the following simple relation [16,41]:

$$\kappa = (2\pi/\lambda)\sqrt{\frac{\varepsilon_{eff}\,\varepsilon_{metal}}{\varepsilon_{eff} + \varepsilon_{metal}}} \pm \kappa_i \quad (2)$$

where the period of LSFLs equals $2\pi/\kappa$, and varies with ε_{eff}.

Using Eq. (2), we calculate the possible periods of small- and large-scale LSFLs as a function of volume fraction of Ni inclusion (f), as shown in Fig. 5. With the period ranges of LSFLs measured from Fig. 3(b), (d),

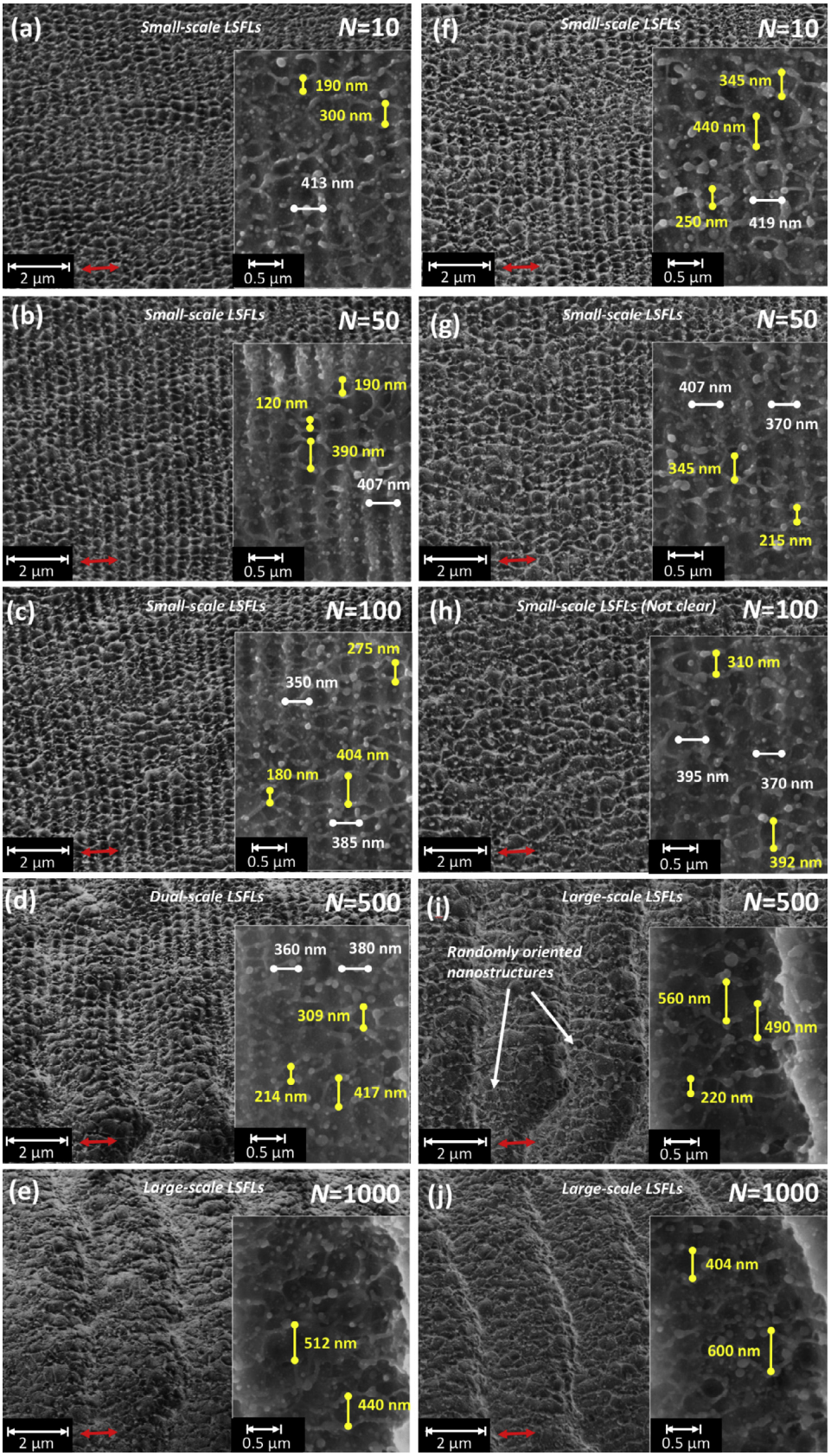

Fig. 3. SEM images of LSFLs on Ni produced at an incident angle of 65° with N irradiating pulses at a laser fluence of 0.17 J/cm^2 [(a)–(e)] and 0.24 J/cm^2 [(f)–(j)]. Double-headed arrows (red) indicate the orientation of polarization. The periods of small-scale LSFLs and nanoscale quasiperiodic structures are denoted in the insets.

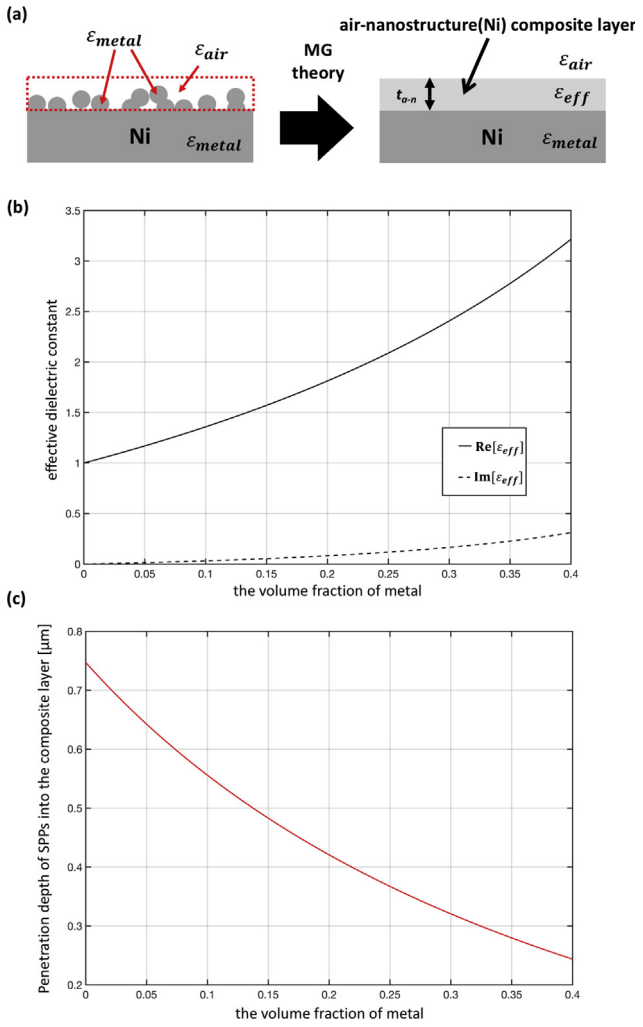

Fig. 4. (a) Sketch of air-nanostructure composite layer in our experiment. (b) Effective dielectric constant and (c) thickness of air-nanostructure composite layer ($t_{a\text{-}n}$) as a function of the volume fraction of Ni inclusion estimated by the Maxwell-Garnett (MG) theory.

and (e), the volume fraction of Ni is expected to be in the ranges of 0.07–0.18 for small- and dual-scale LSFLs and 0.1–0.16 for large-scale LSFLs, described as the blue stripes in Fig. 5.

To directly evaluate the volume fraction of Ni inclusion, first of all the thickness of air-nanostructure composite layer ($t_{a\text{-}n}$) shown in Fig. 4(a) needs to be defined. In fact, the field amplitude of SPPs decays exponentially with a distance from the interface [40], and therefore it is reasonable to define $t_{a\text{-}n}$ as the penetration depth of the air-nanostructure composite layer, where the field amplitude of SPPs falls off a $1/e$ of its amplitude at the bulk Ni surface. By considering the effective dielectric constant of air-nanostructure composite layer in Fig. 4(b), $t_{a\text{-}n}$ is calculated as a function of f in Fig. 4(c) [40]. Then, the morphological profiles (MP) of all three scales of LSFLs are measured by AFM under our experimental conditions used in Fig. 3(b), (d), (e). The MPs of all three LSFLs consist of 256 by 256 pixels describing the height of structures. For all three scales of LSFLs, the volume of Ni in the layer is measured by extracting 256 lines of surface profiles. To reduce the error of estimated volume resulting from the groove of large-scale LSFLs, the interface between the bulk Ni and the composite layer is carefully obtained using the lowest point of each surface profile along the width axis described in Fig. 6. Also, $t_{a\text{-}n}$ and f are determined by using an iterative method so that these values are consistent with Fig. 4(c).

The volume fractions of all small-, dual-, and large-scales of LSFLs estimated from AFM measurements are 0.14 ± 0.033, 0.135 ± 0.040,

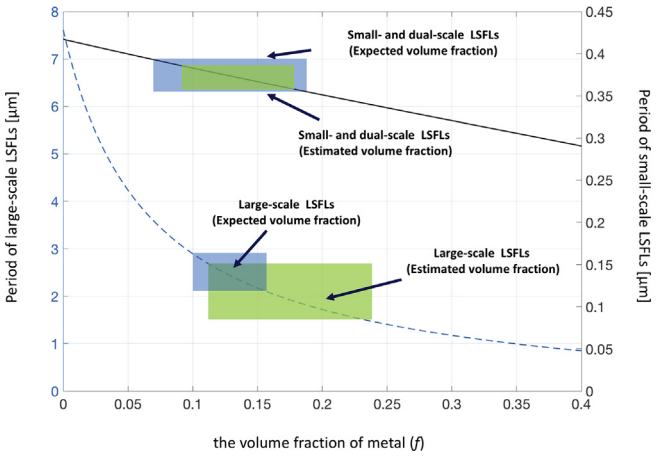

Fig. 5. Periods of small- and large-scale LSFLs versus the volume fraction of metal. The solid and dashed curve denote the calculated periods of small- and large-scale period of LSFLs. The blue stripes indicate the observed periods of small- and large-scale LSFLs, corresponding to the range of volume fraction predicted from the Maxwell-Garnett theory, whereas the green stripes indicate the estimated volume fractions of nanostructures from small-, dual-, and large-scale LSFLs calculated from AFM measurements and describe the corresponding periods at these estimated volume fractions.

and 0.184 ± 0.058, respectively, as shown in Fig. 6. These volume fractions share clearly with the range of volume fraction forecasted by the Maxwell-Garnett theory, as shown in Fig. 5. It is worth noting that f in Fig. 6(c) is a bit overestimated due to large variation of surface profiles along the width axis near the origin of the length axis described in Fig. 6(c). Simply excluding a range of 0–0.5 μm in the length axis reduces f to 0.169 ± 0.058. Consequently, we suggest that both small- and large-scale of LSFLs' formations can be understood by the interference between the incident light and SPPs at the air-nanostructure composite layer and bulk metal rather than air-metal interface.

Next, to understand why dual-scale LSFLs do not exist at a relatively high fluence of 0.24 J/cm^2, we need to take into account the change in reflectance by irradiating fs laser pulses. In fact, following fs laser pulse irradiation, the reflectance of metal surface tends to decrease significantly with the creation of laser-induced nano- and micro-scale surface structures [42], and the size of the structures becomes larger [34]. Therefore, even though small-scale LSFLs form at low pulse numbers, small-scale LSFLs cannot last with more pulses of irradiation, since the absorbed laser fluence monotonically increases with the pulse number. The small-scale LSFLs are effectively blurred by the formation of bigger randomly oriented structures, covering large-scale LSFLs.

Lastly, we would like to briefly note that a larger amount of energy can be required to produce larger-scale LSFLs, since a larger amount of material ablation is requisite. This is why the formation of large-scale LSFLs requires more irradiating pulses and higher fluence than the small-scale ones.

4. Conclusion

In conclusion, following fs laser pulse irradiation, the manipulation of morphological profile of fs LSFLs has been investigated on metals. By increasing the number of irradiating fs laser pulses at large incident beam angles, we have fabricated three types of LSFLs, small-, dual-, and large-scale LSFLs, and observed two kinds of structural period variations, the sequential structural variations from small- to dual- to large-scale LSFLs and the nonsequential variation directly from small- to large-scale LSFLs, depending on the laser fluence. Therefore, with a proper use of these structural period variations, it is expected that changing the incident angle can be fully used to adjust and expand the period and its range of LSFLs, respectively. Moreover, our study has also

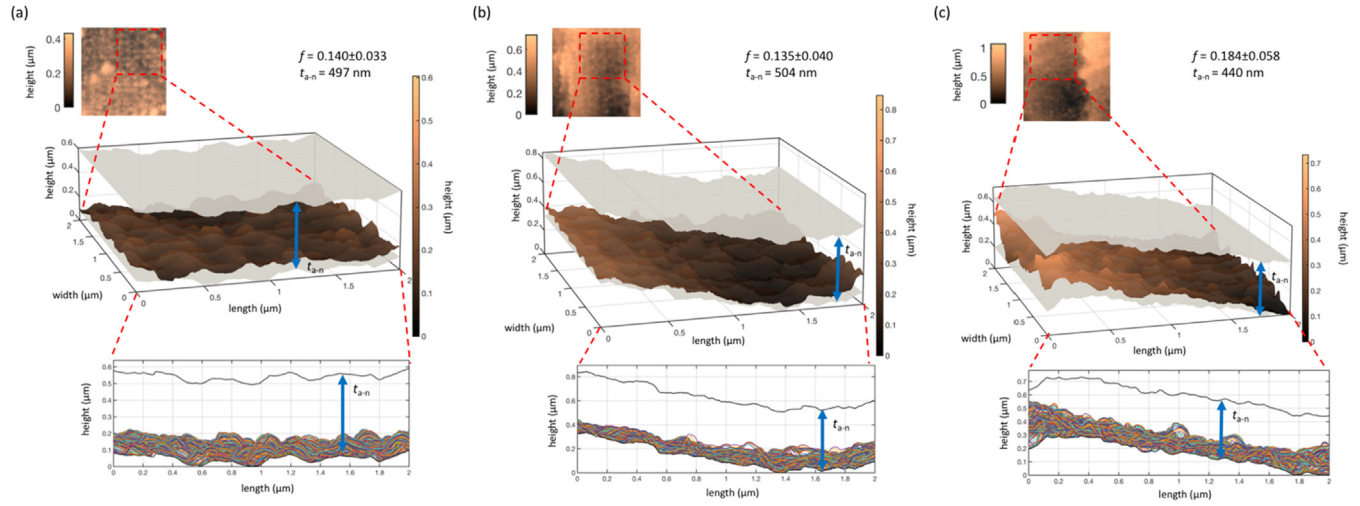

Fig. 6. AFM images of (a) small-, (b) dual-, and (c) large-scale LSFLs produced at $F = 0.17$ J/cm^2. The region between two gray sheets in each AFM image denotes the air-nanostructure composite layer. The volume fractions of Ni inclusion (f) and the thickness of the layer ($t_{a\text{-}n}$) in the figures are calculated from these 3-dimensional AFM measurements in the middle of each figure. The height versus length plots show 256 surface profiles obtained from the AFM measurements projected onto the height-length plane.

shown that these three types of LSFLs can be described by the interference between the incident beam and SPPs at the air-nanostructure composite and metal interface rather than the air-metal interface.

Acknowledgements

This work was supported by the Ministry of Planning and Budget, Korea Institute of Industrial Technology (EO180024). We thank T.K. Lee and H.J. Kim at Korea Institute of Industrial Technology for technical assistance.

References

[1] M. Birnbaum, Semiconductor surface damage produced by ruby lasers, J. Appl. Phys. 36 (1965) 3688 Doi 10.1063/1.1703071.
[2] F. Keilmann, Laser-driven corrugation instability of liquid metal surfaces, Phys. Rev. Lett. 51 (1983) 2097–2100, http://dx.doi.org/10.1103/PhysRevLett. 51.2097.
[3] J.E. Sipe, J.F. Young, J.S. Preston, H.M. van Driel, Laser-induced periodic surface structure. I. Theory, Phys. Rev. B. 27 (1983) 1141, http://dx.doi.org/10.1103/PhysRevB.27.1141.
[4] A.M. Bonch-Bruevich, Surface electromagnetic waves in optics, Opt. Eng. 31 (1992) 718, http://dx.doi.org/10.1117/12.56133.
[5] A. Borowiec, H.K. Haugen, Subwavelength ripple formation on the surfaces of compound semiconductors irradiated with femtosecond laser pulses Subwavelength ripple formation on the surfaces of compound semiconductors irradiated with femtosecond laser pulses, Appl. Phys. Lett. 4462 (2003) 13–16, http://dx.doi.org/10.1063/1.1586457.
[6] S.E. Clark, D.C. Emmony, Ultraviolet laser induced periodic surface structures, Phys. Rev. B. 40 (1989) 2031–2041 http://link.aps.org/abstract/PRB/v40/p2031.
[7] J.F. Young, J.E. Sipe, H.M. Van Driel, Laser-induced periodic surface structure. III. Fluence regimes, the role of feedback, and details of the induced topography in germanium, Phys. Rev. B. 30 (1984) 2001–2015, http://dx.doi.org/10.1103/PhysRevB.30.2001.
[8] Y. Shimotsuma, P.G. Kazansky, J. Qiu, K. Hirao, Self-organized nanogratings in glass irradiated by ultrashort light pulses, Phys. Rev. Lett. 91 (2003) 247405, http://dx.doi.org/10.1103/PhysRevLett. 91.247405.
[9] J. Bonse, J.M. Wrobel, J. Krüger, W. Kautek, Ultrashort-pulse laser ablation of indium phosphide in air, Appl. Phys. A Mater. Sci. Process. 72 (2001) 89–94, http://dx.doi.org/10.1007/s003390000596.
[10] V.R. Bhardwaj, E. Simova, P.P. Rajeev, C. Hnatovsky, R.S. Taylor, D.M. Rayner, P.B. Corkum, Optically produced arrays of planar nanostructures inside fused silica, Phys. Rev. Lett. 96 (2006) 57404, http://dx.doi.org/10.1103/PhysRevLett. 96.057404.
[11] J. Bonse, S. Höhm, S.V. Kirner, A. Rosenfeld, J. Krüger, Laser-induced periodic surface structures – a scientific evergreen, IEEE J. Sel. Top. Quantum Electron. 23 (2017) 109–123, http://dx.doi.org/10.1109/JSTQE.2016.2614183.
[12] R. Buividas, M. Mikutis, S. Juodkazis, Surface and bulk structuring of materials by ripples with long and short laser pulses: recent advances, Prog. Quantum Electron. 38 (2014) 119–156, http://dx.doi.org/10.1016/j.pquantelec.2014.03.002.
[13] A. Weck, T.H.R. Crawford, D.S. Wilkinson, H.K. Haugen, J.S. Preston, Ripple formation during deep hole drilling in copper with ultrashort laser pulses, Appl. Phys. A 89 (2007) 1001–1003, http://dx.doi.org/10.1007/s00339-007-4203-6.
[14] J. Bonse, J. Krüger, S. Höhm, A. Rosenfeld, Femtosecond laser-induced periodic surface structures, J. Laser Appl. 24 (2012) 42006, http://dx.doi.org/10.2351/1.4712658.
[15] A.Y. Vorobyev, V.S. Makin, C. Guo, Periodic ordering of random surface nanostructures induced by femtosecond laser pulses on metals, J. Appl. Phys. 101 (2007) 34903, http://dx.doi.org/10.1063/1.2432288.
[16] T.Y. Hwang, C. Guo, Angular effects of nanostructure-covered femtosecond laser induced periodic surface structures on metals, J. Appl. Phys. 108 (2010) 73523, http://dx.doi.org/10.1063/1.3487934.
[17] J. Bonse, A. Rosenfeld, J. Kruger, On the role of surface plasmon polaritons in the formation of laser-induced periodic surface structures upon irradiation of silicon by femtosecond-laser pulses, J. Appl. Phys. 106 (2009) 104910–104915 http://link.aip.org/link/?JAP/106/104910/1.
[18] M. Huang, F. Zhao, Y. Cheng, N. Xu, Z. Xu, Origin of laser-induced near-subwavelength ripples: interference between surface plasmons and incident laser, ACS Nano 3 (2009) 4062–4070, http://dx.doi.org/10.1021/nn900654v.
[19] T.J.-Y. Derrien, R. Koter, J. Krüger, S. Höhm, A. Rosenfeld, J. Bonse, Plasmonic formation mechanism of periodic 100-nm-structures upon femtosecond laser irradiation of silicon in water, J. Appl. Phys. 116 (2014) 74902, http://dx.doi.org/10.1063/1.4887808.
[20] X.-F. Li, C.-Y. Zhang, H. Li, Q.-F. Dai, S. Lan, S.-L. Tie, Formation of 100-nm periodic structures on a titanium surface by exploiting the oxidation and third harmonic generation induced by femtosecond laser pulses, Opt. Express 22 (2014) 28086–28099, http://dx.doi.org/10.1364/OE.22.028086.
[21] G.D. Tsibidis, A. Mimidis, E. Skoulas, S.V. Kirner, J. Krüger, J. Bonse, E. Stratakis, Modelling periodic structure formation on 100Cr6 steel after irradiation with femtosecond-pulsed laser beams, Appl. Phys. A 124 (2018) 27, http://dx.doi.org/10.1007/s00339-017-1443-y.
[22] F. Garrelie, J.-P. Colombier, F. Pigeon, S. Tonchev, N. Faure, M. Bounhalli, S. Reynaud, O. Parriaux, Evidence of surface plasmon resonance in ultrafast laser-induced ripples, Opt. Express 19 (2011) 9035, http://dx.doi.org/10.1364/OE.19.009035.
[23] A.A. Ionin, S.I. Kudryashov, S.V. Makarov, A.A. Rudenko, L.V. Seleznev, D.V. Sinitsyn, E.V. Golosov, Y.R. Kolobov, A.E. Ligachev, “Heterogeneous” versus “homogeneous” nucleation and growth of microcones on titanium surface under UV femtosecond-laser irradiation, Appl. Phys. A 116 (2014) 1133–1139, http://dx.doi.org/10.1007/s00339-013-8196-z.
[24] D. Dufft, A. Rosenfeld, S.K. Das, R. Grunwald, J. Bonse, D. Dufft, A. Rosenfeld, S.K. Das, R. Grunwald, J. Bonse, Femtosecond laser-induced periodic surface structures revisited : a comparative study on ZnO, J. Appl. Phys. 34908 (2015) 34908, http://dx.doi.org/10.1063/1.3074106.
[25] J. Reif, F. Costache, M. Henyk, S.V. Pandelov, Ripples revisited: non-classical morphology at the bottom of femtosecond laser ablation craters in transparent dielectrics, Appl. Surf. Sci. 197–198 (2002) 891–895, http://dx.doi.org/10.1016/S0169-4332(02)00450-6.
[26] C.S.R. Nathala, A. Ajami, A.A. Ionin, S.I. Kudryashov, S.V. Makarov, T. Ganz, A. Assion, W. Husinsky, Experimental study of fs-laser induced sub-100-nm periodic surface structures on titanium, Opt. Express 23 (2015) 5915–5929, http://dx.doi.org/10.1364/OE.23.005915.
[27] A.A. Ionin, S.I. Kudryashov, A.E. Ligachev, S.V. Makarov, L.V. Seleznev, D.V. Sinitsyn, Nanoscale cavitation instability of the surface melt along the grooves of one-dimensional nanorelief gratings on an aluminum surface, JETP Lett. 94 (2011) 266, http://dx.doi.org/10.1134/S0021364011160065.
[28] G.D. Tsibidis, E. Stratakis, P.A. Loukakos, C. Fotakis, Controlled ultrashort-pulse

laser-induced ripple formation on semiconductors, Appl. Phys. A (2013) 1–12, http://dx.doi.org/10.1007/s00339-013-8113-5.
[29] C.A. Zuhlke, G.D. Tsibidis, T. Anderson, E. Stratakis, G. Gogos, R. Dennis, C.A. Zuhlke, G.D. Tsibidis, T. Anderson, E. Stratakis, G. Gogos, D.R. Alexander, Investigation of femtosecond laser induced ripple formation on copper for varying incident angle, AIP Adv. 8 (2018) 15212, http://dx.doi.org/10.1063/1.5020029.
[30] A.A. Ionin, S.I. Kudryashov, S.V. Makarov, A.A. Rudenko, L.V. Seleznev, D.V. Sinitsyn, V.I. Emel'yanov, Nonlinear optical dynamics during femtosecond laser nanostructuring of a silicon surface, Laser Phys. Lett. 12 (2015) 25902, http://dx.doi.org/10.1088/1612-2011/12/2/025902.
[31] A.A. Ionin, S.I. Kudryashov, S.V. Makarov, L.V. Seleznev, D.V. Sinitsyn, E.V. Golosov, O.A. Golosova, Y.R. Kolobov, A.E. Ligachev, Femtosecond laser color marking of metal and semiconductor surfaces, Appl. Phys. A 107 (2012) 301–305, http://dx.doi.org/10.1007/s00339-012-6849-y.
[32] H.U. Lim, J. Kang, C. Guo, T.Y. Hwang, Femtosecond laser-induced dual periodic structures on Ni, in: Front. Opt. 2017, Optical Society of America, Washington, D.C., 2017: p. JTu3A.41. 10.1364/FIO.2017.JTu3A.41.
[33] V.P. Korol'kov, A.A. Ionin, S.I. Kudryashov, L.V. Seleznev, D.V. Sinitsyn, R.V. Samsonov, A.I. Maslii, A.Z. Medvedev, B.G. Gol'denberg, Surface nanostructuring of Ni/Cu foilsby femtosecond laser pulses, Quantum Electron. 41 (2011) 387–392, http://dx.doi.org/10.1070/QE2011v041n04ABEH014464.
[34] A.Y. Vorobyev, C. Guo, Femtosecond laser nanostructuring of metals, Opt. Express 14 (2006) 2164, http://dx.doi.org/10.1364/OE.14.002164.
[35] T.Y. Hwang, A.Y. Vorobyev, C. Guo, Ultrafast dynamics of femtosecond laser-induced nanostructure formation on metals, Appl. Phys. Lett. 95 (2009) 123111 http://link.aip.org/link/?APL/95/123111/1.
[36] S.I. Kudryashov, S.V. Makarov, A.A. Ionin, C.S.R. Nathala, A. Ajami, T. Ganz, A. Assion, W. Husinsky, Dynamic polarization flip in nanoripples on photoexcited Ti surface near its surface plasmon resonance, Opt. Lett. 40 (2015) 4967–4970, http://dx.doi.org/10.1364/OL.40.004967.
[37] M.A. Ordal, L.L. Long, R.J. Bell, S.E. Bell, R.R. Bell, R.W. Alexander, C.A. Ward, Optical properties of the metals Al Co, Cu, Au, Fe, Pb, Ni, Pd, Pt, Ag, Ti, and W in the infrared and far infrared, Appl. Opt. 22 (1983) 1099, http://dx.doi.org/10.1364/AO.22.001099.
[38] T.C. Choy, Effective Medium Theory: Principles and Applications, Oxford University Press Inc., New York, 1999.
[39] J.C.M. Garnett, Colours in metal glasses and in metallic films, Philos. Trans. R. Soc. Lond. Ser. A Contain. Pap. A Math. Phys. Charact. 203 (1904) 385, http://dx.doi.org/10.1098/rsta.1904.0024.
[40] S.A. Maier, Plasmonics: Fundamentals and Applications, Springer, New York, 2007.
[41] J.E. Sipe, New Green-function formalism for surface optics, J. Opt. Soc. Am. B. 4 (1987) 481–489, http://dx.doi.org/10.1364/JOSAB.4.000481.
[42] A.Y. Vorobyev, C. Guo, Enhanced absorptance of gold following multipulse femtosecond laser ablation, Phys. Rev. B. 72 (2005) 195422, http://dx.doi.org/10.1103/PhysRevB.72.195422.